CORE
Metadata, citation and similar papers at core.ac.uk
Provided by Digital Commons @ West Chester University

West Chester University
Digital Commons @ West Chester University

Chemistry
College of Arts & Sciences

2008

Wet Etching of Pillar-Covered Silicon Surfaces: Formation of Crystallographically Defined Macropores

M E. Dudley

Kurt Kolasinski
West Chester University, kkolasinski@wcupa.edu

Follow this and additional works at: http://digitalcommons.wcupa.edu/chem_facpub

Part of the Chemistry Commons

Recommended Citation
Dudley, M. E., & Kolasinski, K. (2008). Wet Etching of Pillar-Covered Silicon Surfaces: Formation of Crystallographically Defined Macropores. *Journal of the Electrochemical Society, 155*(3) http://dx.doi.org/10.1149/1.2826292

This Article is brought to you for free and open access by the College of Arts & Sciences at Digital Commons @ West Chester University. It has been accepted for inclusion in Chemistry by an authorized administrator of Digital Commons @ West Chester University. For more information, please contact wcressler@wcupa.edu.

Journal of The Electrochemical Society, **155** (3) H164-H171 (2008)
0013-4651/2008/155(3)/H164/8/$23.00 © The Electrochemical Society

Wet Etching of Pillar-Covered Silicon Surfaces: Formation of Crystallographically Defined Macropores

Margaret E. Dudley* and Kurt W. Kolasinski,z**

Department of Chemistry, West Chester University, West Chester, Pennsylvania 19383, USA

Silicon substrates exposed to laser ablation in a chemically reactive environment such as SF_6 or HCl can experience spontaneous formation of conical pillars. We use these pillars as a template to define the dimensions and order of macropores produced by etching such substrates in aqueous solutions of KOH or tetramethylammonium hydroxide. The pillars anchor the sidewalls of the pores during etching, and the interpillar spacing controls the width of the pores. The macropores have crystallographically defined shapes for which we develop an explanation based on the kinetics of etching. Si(001) macropores can be etched such that they are rectangular with straight walls and an inverted pyramidal bottom. They have been etched as through holes, which is of interest for optical applications. On Si(111), there is a transition from hexagonal to triangular macropores that are all aligned in one direction. The Si(111) pores exhibit an optimum etch time before they begin to disappear. The behavior of the macropores is quite similar regardless of whether the pillars are produced by nanosecond or femtosecond lasers. Differences observed relate to the different initial structures (spacing and regularity) of these two different types of pillar-covered surfaces.
© 2008 The Electrochemical Society. [DOI: 10.1149/1.2826292] All rights reserved.

Manuscript submitted October 9, 2007; revised manuscript received November 14, 2007. Available electronically January 2, 2008.

There is increasing awareness of a new variant of synthetic chemistry that strives not so much to create a desired molecule/composition, but rather, that seeks to make a desired architecture. Impetus for this derives from the observation that, particularly on the nanoscale, the properties of materials change with the size of the sample. Thus, for instance, the substantial interest in nanowires/tubes,[1-3] porous solids,[4-6] and metallorganic framework compounds,[7-9] which are examples of nanomaterials created by etching and growth. With a particular interest in silicon, we have embarked on a series of studies aimed at elucidating the dynamics of and determining the versatility of structural transformations by means of (laser-assisted) chemical processes beginning with solid substrates.[10]

Silicon undergoes radical changes as a result of being restructured. Etching to create nanocrystalline silicon leads to quantum confinement of both electrons and phonons. This in turn facilitates the observation of strong visible photoluminescence and even optical gain[11-15] from a material that is normally an abysmally weak emitter in the bulk phase,[16] unless it is, for example, specially pumped to produce a Raman laser.[17-19] When covered with pillars produced by chemically enhanced laser ablation, polished Si changes from a shiny grayish mirror into a black material with virtually no reflectivity even below the bandgap.[20,21] Pillars can be created by either nanosecond or femtosecond laser pulses. Here we denote pillars made with a nanosecond laser as nanosecond pillars; similarly, femtosecond pillars are those pillars produced with a femtosecond pulsed laser.

Pillars form as the result of the combination of laser ablation, etching, and growth.[10] Although both nanosecond and femtosecond pillar-covered surfaces are black and the structures are roughly conical, there are significant differences in the structures of the postirradiation substrates. Nanosecond pillars produced in SF_6 are solid core, crystalline, and surrounded by deep circular holes, which form as a precursor to the pillars. The pillars are initially $\sim$50 to > 100 μm tall and their tips extend ≥ 10 μm above the plane of the pristine substrate. The spacing between the pillars is $\sim$15 μm and does not respond to the wavelength of nanosecond light.[10] Femtosecond pillars produced in SF_6 exhibit substantial porosity in an outer layer that covers a much smaller solid crystalline core.[22] Their height is usually in the range of 10–20 μm, and the formation of holes does not precede their formation. Their tips are at or below the initial surface. The interpillar spacing is $\sim$7–10 μm (changing with number of shots and laser fluence) when produced with 800 nm light, and this spacing responds to the wavelength of the femtosecond light.[23]

It has long been recognized that the etching of silicon in aqueous solutions can be anisotropic and, therefore, that it can be used to identify crystal defects based on characteristic etch shapes.[24-26] Anisotropic etching of nominally flat silicon surfaces has grown in importance since it was realized that it can be used to reduce the reflectivity of the surfaces in solar cells.[27-30] As discussed by Hilali et al.[31] and Ruby et al.,[32] texturing is a vital step in the fabrication of high-efficiency silicon solar cells. The reflectivity reduction is not merely the consequence of surface roughening; rather, it occurs because of specific crystallographically defined roughening, which leads to the formation of pyramidal structures with an appropriate sidewall angle such that photons are not easily backscattered from the surface.

The chemistry of silicon etching in alkaline solutions has been intensively studied.[33,34] Crystallographically anisotropic etch rates are believed to be related to the ease with which a pentacoordinated transition state can be formed during nucleophilic attack by OH^- on a hydrogen-terminated surface Si atom.[35,36]

Apart from how it affects optical and electronic properties, there is also interest in surface structuring in relation to a number of biochemical problems.[37,38] Essentially, every cell in a body, with the exception of blood cells, is only viable when in contact with a surface. The life cycle of cells responds to a range of chemical and surface topological clues.[39] The development of methods by which we can controllably change surface topography, porosity, and chemistry will help us to disentangle how surface related cues affect cell growth, differentiation, propagation, apoptosis, and necrosis.

Here we report on studies that combine wet etching with laser ablation to determine the range of structures that can be formed. Studies into the sharpening of laser pillars will be reported elsewhere. In this report, we concentrate on the macropores that are created when laser-ablation-produced pillars are overetched. This method leads to a form of macroporous silicon with a narrow pore size distribution that is determined by the initial interpillar spacing. The combination of wet etching with previously developed techniques to vary the interpillar spacing[23] will lead to a method of producing macropores with a mean pore size that is under the control of the experimentalist.

As far as the etchant is concerned, we demonstrate that the anisotropy is the most important parameter. For all compositions studied, the Si{111} planes etch most slowly; however, by changing composition and temperature, we can change the relative etch rate of the {110} and {100} planes. We denote as class 1 etchants in which the {110} planes are faster etching and as class 2 those in which the {100} planes are faster etching. Any etchant of a given class will

* Electrochemical Society Student Member.
** Electrochemical Society Active Member.
z E-mail: kkolasinski@wcupa.edu

Downloaded on 2013-12-02 to IP 144.26.117.20 address. Redistribution subject to ECS license or copyright; see ecsdl.org/site/terms_use

produce the same structures, although some do it more rapidly than others because they have a higher etch rate. Etchant anisotropy, the amount of silicon removed, and Si substrate crystallography are the most important parameters for determining the macropore morphology.

Experimental

Si(001) and Si(111) wafers (p-type) were cleaved into 1 cm^2 pieces. Si pillars were produced by means of chemically enhanced laser ablation using either nanosecond[40,41] or femtosecond[23,42] lasers in a manner described in more detail elsewhere. After ultrasonic cleaning in acetone and methanol, the substrates were placed inside a vacuum chamber with a base pressure of ~1 mbar and subsequently laser processed in ~400 mbar of SF_6. Femtosecond pillars were produced with normally incident ~1 mJ cm^{-2} pulses of 800 nm/130 fs light at a repetition rate of 1 kHz from a regeneratively amplified Spectra Physics Ti-sapphire laser system. The samples were scanned with typically four single scan lines and rotated orthogonally for an additional four single scan lines. This resulted in ~16 easily identifiable intersections where the sample had been scanned twice. These intersections allowed us to probe the same area before and after chemical treatments. Nanosecond pillars were produced with a Lambda Physics LPX105 operating on the XeCl excimer (308 nm, ~3 mJ cm^{-2} per pulse, 20 ns pulse width, 20 Hz repetition rate). Single scan lines were used in this case. Substrate scan rates were adjusted so that the irradiated areas were exposed to several hundred laser shots for complete pillar development.

Samples were annealed for 2–5 h usually at 1200°C in an ambient atmosphere. This step was not important for macropore formation, and these conditions are only reported for completeness. Annealing was performed because it was important when attempting to sharpen pillars. Those results will be reported elsewhere.

We specifically chose potassium hydroxide (KOH) and tetramethylammonium hydroxide (TMAH) and the compositions listed below so that we could make direct comparisons to the etch rate data of Wind and Hines,[43] Wind et al.,[44] and Zubel and Kramkowska[45,46] for mechanistic insights. To facilitate comparisons, we report compositions in the units used in these references. Samples etched in TMAH were etched in a 25 wt % solution at 60°C. Samples treated with KOH were etched in solutions of either 25 wt %, 45 wt %, or 50 w/v % at temperatures of 60 or 70°C. All these were class 1 etchants. A few samples were also etched in 12.5 w/v % KOH + isopropanol (IPA), which is a class 2 etchant, and a 20 wt % TMAH + 20 v % IPA at 60°C (class undetermined). Etching of femtosecond pillars was performed in an isothermal bath with temperature control to better than ±1°C. Because TMAH or KOH etch SiO_2 very slowly, the oxide layer was stripped off by a 4 min etch in 5 wt % HF before etching in basic solutions. On some early samples, this was not done and they therefore required much longer etching times to remove the same amount of silicon. Etching was often performed in multiple steps, for which we used the notation 15 + 5 min to indicate a 15 min etch followed by a 5 min etch. Imaging was performed with an FEI Tecnai T12T scanning electron microscope (SEM), typically at a voltage of 5 kV with a working distance of ~15 mm.

Results

Nanosecond macropores.— The results of etching nanosecond pillars were reported briefly elsewhere[41,47] and are summarized here. With nanosecond pillars, all etching was carried out at ~80°C in roughly 40 wt % KOH. At the time, we did not think these parameters were critical so we did not attempt to control them precisely. The mechanism of pillar production[10] with nanosecond lasers is such that deep (up to ~100 μm) holes surround each pillar. Because of the presence of these round holes, we anticipated that overetching of the nanosecond pillars would lead to macropore formation and it was indeed what we discovered.[47] Si(001) pillar-covered substrates etch to reveal rectangular macropores with widths of 13–17 μm. The pore width is somewhat smaller than the interpillar spacing, which makes sense since some of the space between the pillars must be used as part of the pore walls. Rectangular pores with {100} walls are observed though on occasion they are observed to be overlapped with {110} pores, which are rotated 45° with respect to {100} macropores, to create an octagonal morphology. We were able to etch these pores completely through the wafer. Si(111) pillar-covered substrates etch to reveal rounded pores with triangular bottoms. The 17–20 μm width is again related to the interpillar spacing.

Si(100) macropores.— We began investigating the wet etching of femtosecond pillars in an effort to sharpen the tips to nanoscale proportions as demonstrated previously for nanosecond pillars.[41] We did not anticipate the formation of macropores due to the lack of holes that occur in the space between the pillars. To our surprise, macropores are readily formed. The pillars anchor the incipient walls of the macropores. They appear to resist etching compared to the spaces between the pillars, which readily etch away to reveal, first, rounded pores and then crystallographically defined pores. The etching of the interpillar regions is much faster than the etching of the pillars themselves, which indicates that the interpillar regions must be highly defective and perhaps somewhat porous as a result of the laser processing. The structural transitions are displayed in Fig. 1 for Si(001).

In all of the solutions used, the etch rate of the {111} planes is significantly less than all other planes. As Fig. 1 demonstrates, when a pillar-covered Si(001) substrate is etched in a KOH or a TMAH solution for which the {110} planes are etched significantly faster than the {001} planes, the substrate develops square macropores with a width of ~4 μm. Again, this is somewhat smaller than the spacing between the pillars. Using image processing to count the density of pillar tips prior to etching, the mean distance between pillars is 8.1 ± 0.5 μm. The sidewalls are perpendicular to the (001) plane, and the bottom of the pore exhibits distinct lines that run perpendicular to the sidewalls. The sidewalls are rotated by 45° with respect to the cleavage planes of the Si(001) substrate. The primary axes of the substrate are easily recognized because the substrate is cleaved into a rectangular chip, whose axes run along the ⟨110⟩ directions. The lines at the bottom of the pore form one of three patterns: (*i*) intersecting to form a crosslike pattern, (*ii*) intersecting at the ends of a line, and (*iii*) intersecting at the corners of a rectangle. All three patterns are observed for all etch durations. The sidewalls etch slowly such that the pores gradually get wider and coalescence of pores, at least over a portion of the sidewall, can occur at long etch times. The definition of "long" depends on the etch rate of the solution and whether the oxide layer is removed prior to etching but generally corresponds to times in excess of 10–15 min.

To assign the structure at the bottom of the pore, we cleaved both samples processed with nano- and femtosecond laser pulses and imaged the pores in cross section. We cannot define precisely where a cleave intersects a pore; however, Fig. 2a displays the cross section of what appears to be a nanosecond pore that exhibited a rectangle at the bottom and Fig. 2b an image of a femtosecond pore with a pointed bottom. Some femtosecond pores also exhibit flat bottoms. The assignment of the crystallographic directions is discussed below. The bottom of the pore angles in, toward a flat bottom (corresponding to the rectangle). The angle of the bottom (bottom wall) of the nanosecond pore to the angled walls is 56.5° when the angles of both sides with bottom are taken together in order to average out any uncertainties in the imaging process. In the femtosecond pore, the angled walls make an angle of 54.2° with the [001] direction. The differences are within the uncertainty of the measurements.

The structure revealed in Fig. 1 is not a trivial result. Rectangular macropores with vertical walls are only obtained if the etchant etches {110} planes faster than {100} planes. If a pillar covered Si(001) substrate is etched in a solution for which the etch rates of

Downloaded on 2013-12-02 to IP 144.26.117.20 address. Redistribution subject to ECS license or copyright; see ecsdl.org/site/terms_use

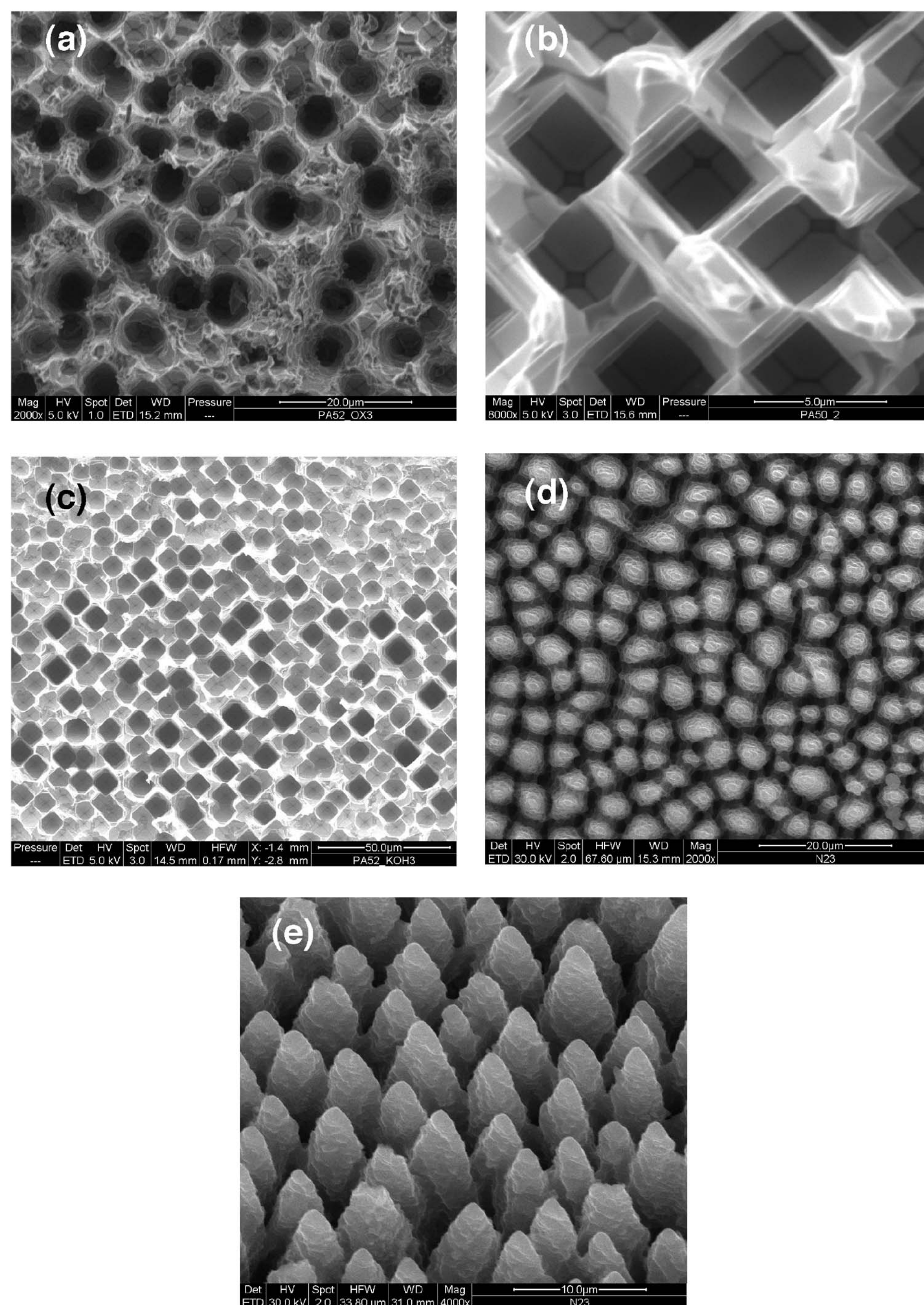

Figure 1. (a, b) Plan view SEM images of Si(001) pore development during wet etching in alkaline solution of an initially femtosecond pillar-covered substrates. The initially round pores in panel (a) transform into rectangular pores as in panel (b) (c) Size distribution of the rectangular pores is rather uniform. For comparison to the initial conditions, we show a pillar-covered substrate before wet etching in (d) plan view and (e) at an inclination of 30°. Note that the scale of (a) and (d), as well as Fig. 3a, are all the same. After laser processing, the substrates were etched as follows: (a) 1 h anneal in air at 1050°C, 7 min 45 wt % KOH 60°C, then 2 h annealed in air at 1200°C, 4 min dip in HF, 2.5 min 45 wt % KOH 60°C. (b) 2 h 1050°C, then 4 h 1200°C annealed in air, 4 min dip in HF, 5 min 25 wt % TMAH 60°C. (c) Same sample as in (a) but with an additional 4 min dip in HF, 3 min 45 wt % KOH 60°C.

the {001} planes are greater than the etch rates of the {110} planes (such as the KOH + IPA solution),[43,44] the macropores do not develop into rectangular pores with straight walls. The bottoms of the pores look similar in both cases. However, when viewed from above the pores appear octagonal with sides along both {001} and {110} directions. Closer inspection reveals that the pore walls are highly inclined and stepped, not vertical. At long etch times when the pores have become shallow depressions, the octagonal shape gives way to squares defined by the ⟨110⟩ directions and then the pores gradually disappear into surface roughness.

Si(111) macropores.— The development of crystallographically defined macropores on initially femtosecond pillar-covered (111) substrates is illustrated in Fig. 3. Round macropores quickly give way to hexagonal pores, Fig. 3a. The hexagons consist of two triangles rotated by 180° with respect to each other. Only one orientation of the triangles survives continued etching. The reason for the selection of only one of the triangles is that the sidewalls change from straight walls containing many steps to flat but inclined planes, Fig. 3b. Only three of the inclined planes survive and develop. Because these are well-defined crystallographic planes, as discussed below, when the walls of neighboring pores intersect they form sharp ridges, as shown in Fig. 4. The tops of the ridges routinely reach widths on the order of 100 nm or less. Regardless of which solution was used, KOH(aq), KOH + IPA, TMAH(aq), or TMAH + IPA, the same structure is formed. The solutions without IPA have a tendency to form smoother ridge structures.

The bottoms of the pores develop a flat geometry. At this point, the bottom of the pore is more or less pinned to a certain depth but the top of the pore continues to etch, much like the etching of Si(001) in KOH + IPA. The pores reach a maximum depth and then

Downloaded on 2013-12-02 to IP 144.26.117.20 address. Redistribution subject to ECS license or copyright; see ecsdl.org/site/terms_use

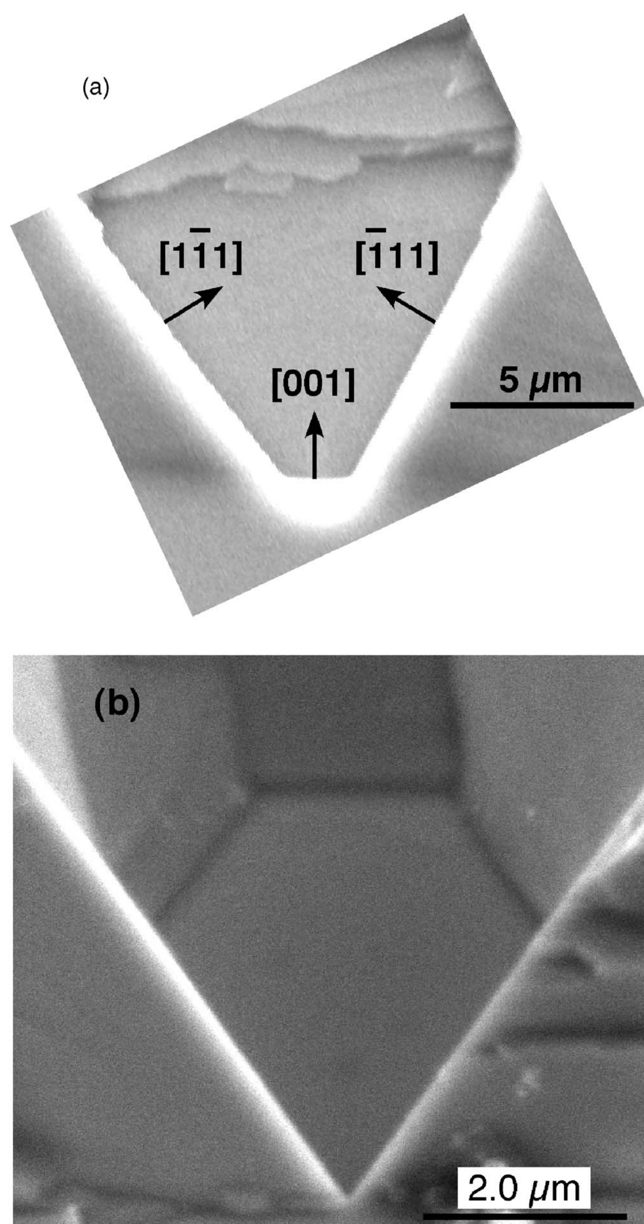

Figure 2. Si(001) macropores shown in cross section: (a) A macropore created by etching nanosecond pillars and (b) a macropore created by etching femtosecond pillars. The angled walls in both cases are of the {111} family of planes and two of which have been semiarbitrarily labeled.

slowly decay, as shown in Fig. 3c. Even longer etch durations lead to the return of mostly flat surfaces. Because of the change in shape and the inclined nature of the sidewalls, the size of the pores changes as etching progresses. The hexagonal pores are ~5 μm across, whereas triangular pores of the type shown in Fig. 3b are ~7 μm on a side. The triangle at the bottom also varies in size from pore to pore and as a function of etching time. The slightly longer sidewalls on Si(111) than Si(001) are related both to the difference in shape as well as the finding that the interpillar spacing of 10.1 ± 0.6 μm is somewhat larger on Si(111).

Discussion

Si(100) macropores.— A Si(100) substrate cleaves easily into a rectangular shape with edges defined by the {110} planes, and this allows us to orient the sample with respect to its crystallographic axes. With the sample cleaved and oriented in this way, it is immediately obvious from Fig. 1 that the pores are rotated by 45° with respect to the {110} planes and that the pore walls descend orthogonally into the substrate. Therefore, the sidewalls have {100} orientation, as can be confirmed by calculating the angle between the normals to these planes with the dot product of the normals. Cross sections of both nano- and femtosecond pores demonstrate that true macropores are formed in that they have widths (~15 or ~4 μm, respectively) that are smaller than the depth of the pore (sometimes in excess of 100 μm). Macropores with walls of exclusively {110} orientation never appeared. Such sides have only been observed in combination with {100} walls. Furthermore, when pores are bounded along the {110} directions, these walls are not straight; rather, they are composed of many steps descending into the substrate.

In the etching literature, there is a simple rule of thumb "fast etching planes disappear and slow etching planes emerge when etching a concave object, whereas slow etching planes disappear and fast etching planes emerge when etching a convex object." We want to test whether this rule of thumb holds in the case of etching pillar-covered surfaces, which exhibit concave topological features between the pillars as well as the convex pillar tips. Because the concave features become the macropores, the sidewalls of the macropores should be determined by the anisotropy of the etchant. Therefore, the pore walls should correspond to the more slowly etching of either the {100} or {110} family of planes. Consistent with this line of reasoning, if we can switch which family of planes etches more slowly, we should be able to switch the orientation of the sidewalls.

Wind and Hines,[43] Wind et al.,[44] and Zubel and Kramkowska[45,46] have measured orientation-dependent Si etch rates in various KOH and TMAH solutions. Both the {100} and {110} planes etch fairly rapidly. Which family of planes etches more rapidly depends on the concentration of alkali, the temperature, and the addition of IPA, and this allows us to make two different classes of etchants:

1. In, for example, 40 wt % KOH at 60°C, 50 w/v % KOH at 70°C and the TMAH solutions without IPA, the {110} family etches much faster than the {100} family.
2. For 12.5 w/v % KOH + IPA at 70°C, the {100} family etches substantially faster than the {110} family.

If the rule of thumb holds, then the two different classes of etchants should each be able to produce vertical walled rectangular pores and the macropores created by class 1 should be rotated by 45° with respect to the macropores created by class 2. The answer is that the rule of thumb holds only partially. Although it is true that rectangular pores with vertical {100} walls develop in solutions that etch {110} planes quickly compared to relatively slow etching {100} walls (class 1 etchants), we are unable to make exclusively {110} walls in etchants for class 2 etchants (in which the {100} etch rate exceeds the {110} etch rate). This may be because the tops of the pores lie in the (001) plane and etching from the top down is just as fast as the etching of the {100} sidewalls, which leads to highly stepped rather than vertical walls.

Determination of the crystallography of the bottom of the pore requires both Fig. 1 and 2. The macropores produced from both nano- and femtosecond pillar-covered surfaces have the same structure at the bottom of the pore. The cross pattern requires that the projections of the normal vectors of the planes that define the bottom of the pore have equal x and y components. Thus, planes of the general form $\{xxy\}$ come into consideration. The cross sections in Fig. 2 show that the bottoms of the pores are parallel to the top of the macroscopic crystal and correspond, therefore, to a (100) plane. The angle between the (100) plane and the inclined bottom walls is 54–56°. Straightforward calculations show that among the stable low index planes that can be expected to occur, only the {111} planes at 54.6° are consistent with both of the geometrical criteria. The (556), (221), and (331) planes lie at 49.7, 70.5, and 76.7°, respec-

Downloaded on 2013-12-02 to IP 144.26.117.20 address. Redistribution subject to ECS license or copyright; see ecsdl.org/site/terms_use

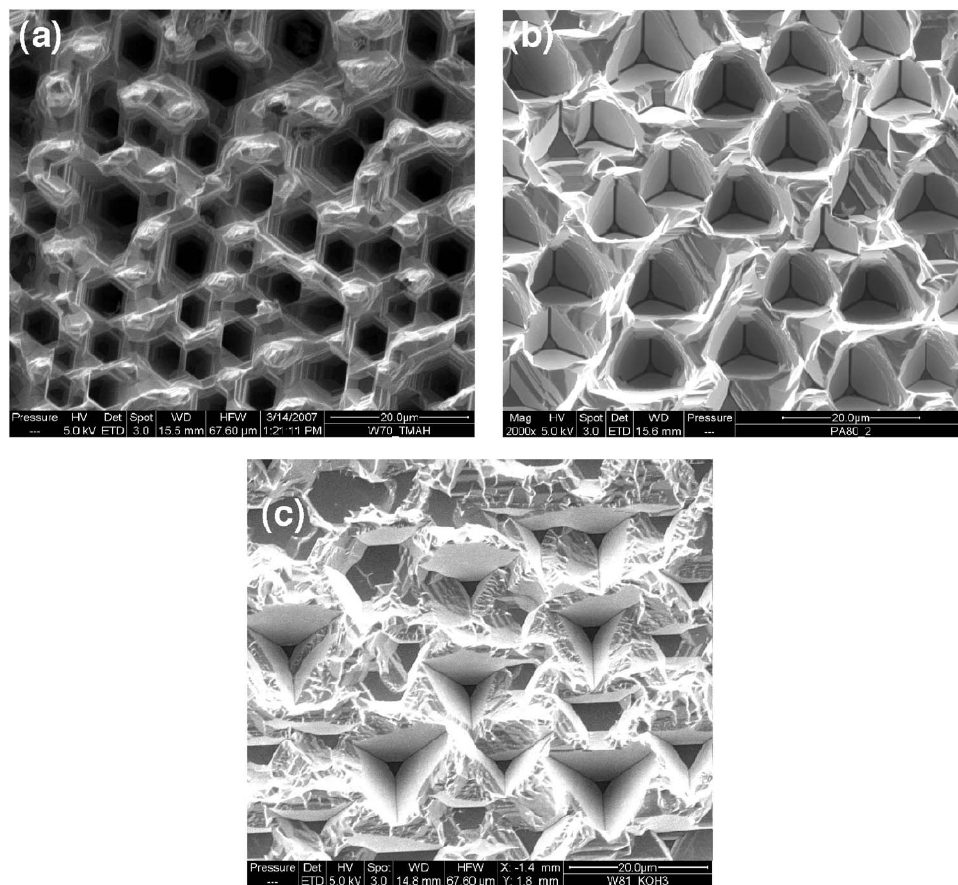

Figure 3. Plan view SEM images of pore development on Si(111) as the result of wet etching in alkaline solution of an initially femtosecond pillar-covered substrate. (a) Initially round pores become hexagonal for a sample that was etched for 15 min in 25 wt % TMAH at 50°C after a 4 h anneal in air at 1200°C and a 4 min dip in HF to remove the oxide. (b) More extensive etching (15 min in 25 wt % KOH at 60°C) causes hexagonal pores to turn triangular regardless of whether KOH or TMAH is used. (c) Heavy etching, 15 + 2 + 5 min in 45 wt % KOH at 70°C, eventually leads to the destruction of the pores. Note that the scale of Fig. 1a and (a) are the same and that the initially pillar-covered substrate looks much like Fig. 1d and e in all cases.

tively, and fall out of consideration. Therefore, we conclude that the bottoms of the Si(001) pores are inverted pyramids with {111} sides as assigned in Fig. 1 and 2.

The geometry of the bottom of the pore is important for the explanation of why etching does not stop once the {111} planes appear and why through holes can be etched. It is possible that the shape of the very bottom of the pore varies between tip and flat or line and flat as etching progresses. A fluctuating geometry at the bottom of the pore would be consistent with our observation that there appears to be no termination to the etching of the Si(001) in depth. In other words, etching continues in the z direction even after the appearance of the {111} planes. {111} planes etch at a much slower rate than {100} planes;[44] thus, the permanent presence of at least a small (001) plane at the bottom of the pore ensures that etching continues in the z direction. The three types of bottoms (tip, flat, or line) appear to be fairly randomly distributed. All three can be seen before the pores have clearly made the transition from irregular rounded pores (Fig. 1a) to rectangular macropores (Fig. 1b). The distinction between tip and line bottoms is somewhat arbitrary; perhaps it is better to say that sometimes the {111} planes are of such vastly different sizes that there is an appreciable line at the bottom, whereas for other pores, the {111} planes are sufficiently close in size that they essentially approximate a tip.

The mechanism of pore formation observed here is distinctly different than pore formation during anodic etching of n-type Si(001) in the dark in acidic fluoride solutions and, therefore, pore formation is not a simple function of crystallography. Anodic etching leads to highly branched rectangular pores with {110} sidewalls

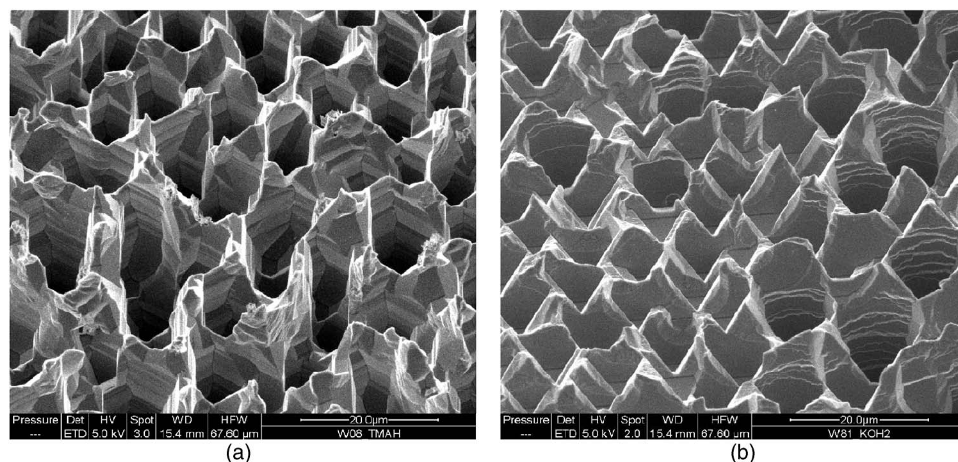

Figure 4. SEM images taken at 30° tilt. Si(111) pores form nanosharp ridges between the pores as the transition from hexagonal to triangular pores occurs. When looked at in plan view, these samples look much like the sample shown in Fig. 3b. Preparation conditions: (a) 4 h annealed in air at 1200°C, 4 min dip in HF, 8 min 25 wt % TMAH 60°C. (b) 5 h annealed in air at 1200°C, 4 min dip in HF, 17 min 45 wt % KOH 70°C.

Downloaded on 2013-12-02 to IP 144.26.117.20 address. Redistribution subject to ECS license or copyright; see ecsdl.org/site/terms_use

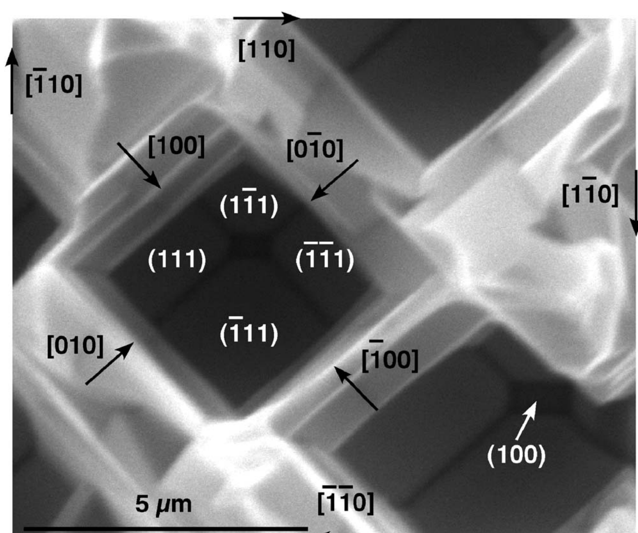

Figure 5. Crystallographic assignment of a Si(001) macropore created from a femtosecond pillar-covered substrate by etching in 40 wt% KOH at 60°C.

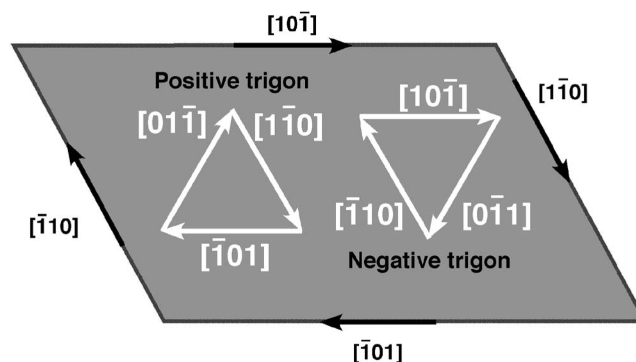

Figure 6. Si(111) cleaves naturally into a parallelogram. One can define two triangles that are rotated with respect to each other by 180° and with two axes parallel to sides of the crystal as shown.

and inverted pyramidal pore tips. For etching in alkaline solutions, we observe pores with inverted pyramidal pore tips but with {100} sidewalls (for class 1 etchants in which the {100} planes etch slowly relative to {110} planes) as shown in Fig. 5. Ross et al.[48] have explained the geometry of anodically etched pores on the basis of a kink atom step-flow etch mechanism at the intersection of the {111} angled walls with the vertical pore wall. The preference for {110} planes is ascribed not to their being particularly stable; rather, because they are the planes that remain after a series of etching events at kink sites, which are twofold coordinated, what Ross et al. identify as $[11\bar{2}]$ steps, in preference to etching at threefold coordinated $[\bar{1}\bar{1}2]$ steps. Obviously, this mechanism is not active in the case of alkaline etching and the mechanism of anodic etching is much different compared to alkaline etching. Their explanation of pore formation of such crystallographically defined pores relies on the etching being dependent on electric field enhancement at the tip of the pyramid because this enhancement aids the transport of the holes that are required to initiate anodic etching. No such field effect is present in the system we are studying.

Si(111) macropores.— Si(111) macropores change shape from hexagons to triangles, which are all aligned with one orientation. A Si(111) crystal cleaves naturally into a parallelogram, or in some unfortunate cases a triangle, with ⟨110⟩ sides, such as that shown in Fig. 6. Two types of parallelogram can be formed because, while the $[\bar{1}10]$ direction is commonly chosen to be one side because this direction corresponds to the wafer flat, the other side can either cleave along the $[10\bar{1}]$ direction as shown or along the $[01\bar{1}]$ direction. There are two triangles, which at first glance appear to be symmetry equivalent, that can be drawn on such a crystal, one that points up and one that points down. The upward-pointing triangle is called a positive trigon as described below in analogy to structures found on natural diamond crystals.[49] The steps along the edges of the positive trigon are all of the $\langle\bar{1}\bar{1}2\rangle$ type. The downward triangle or negative trigon has $\langle 11\bar{2}\rangle$ steps. Even though these two triangles appear to be symmetry equivalent, only one of them (the negative trigon) survives prolonged etching. This must in some way relate to the different step structures because rotating the crystal about a C_2 axis perpendicular to the (111) plane transforms the $[\bar{1}01]$ into the $[10\bar{1}]$ direction and the two trigons are otherwise indistinguishable. As shown below, all of the walls of the Si(111) macropores belong to the {111} family. Therefore, unlike macropores on Si(001), we cannot explain the development of the Si(111) macropores based on wall geometry alone. Instead we must also consider the morphology of the pores edges.

Frank et al.[49] showed that natural diamond exhibits triangular etch features that are centered along lines of dislocation defects, which are nearly perpendicular to the surface. These etch features are called trigons. The upward-pointing trigon points in the direction of the octahedral face of diamond and is called a positive trigon (or a trigon with positive orientation). The downward-pointing triangle is a negative trigon. Frank et al.[49] showed that exclusively negative trigons are observed on natural diamond and that these are the result of etching rather than growth. This is the same orientation we observe in wet etched Si.

The explanation for the exclusive formation of negative trigons in diamond has been formulated by Angus and Dyble.[50] Assuming that during etching the surface of diamond is unreconstructed and that the etch rate of surface atoms depends inversely on the coordination number of the atoms (i.e., fourfold coordinated atoms etch slower than threefold coordinated atoms etc.), then the etch pits that form should be defined by edges with the highest possible coordination. This is because edges composed of low coordination number atoms will etch rapidly and disappear, leaving only edges with the most highly coordinated atoms. More recently, Hines[33] and Flidr et al.[51,52] have developed kinetic Monte Carlo simulations to model and interpret the results of silicon etching experiments carried out in aqueous alkaline and acidic solutions. These simulations specifically incorporate differences in etch rates for each type of site on the surface (e.g., terrace, kink sites, and all the different types of step sites). They also find that the two-dimensional surface structure formed by etching is sensitive to the relative etch rates and that etch pits in terraces and triangularly etched steps are observed when kink sites etch rapidly, but the threefold step sites (called monohydride steps) etch more slowly than either of the two types of twofold coordinated step sites (called dihydride steps).

The coordination of atoms in the (111) plane as well as the three possible trigons formed in the (111) plane are illustrated in Fig. 7. The unreconstructed surface of the (111) plane in a diamond lattice is composed of a bilayer. The upper bilayer atom is threefold coordinated and has one dangling bond. The lower bilayer atom is fourfold coordinated because it is bound not only to the three upper atoms but also to one atom in the next lower bilayer. This is illustrated in Fig. 7a in which the upper bilayer atoms are shaded black and the lower bilayer atoms are the lightest. The atom in the next lowest bilayer is shaded medium gray. A positive trigon is created by forming $\langle\bar{1}\bar{1}2\rangle$ type steps down to the next bilayer in one of two ways. Regardless of whether a positive trigon is created by cutting the (111) lattice along the upper bilayer atoms, as shown in Fig. 7b, or along the lower bilayer atoms, as shown in Fig. 7c, the resulting

Downloaded on 2013-12-02 to IP 144.26.117.20 address. Redistribution subject to ECS license or copyright; see ecsdl.org/site/terms_use

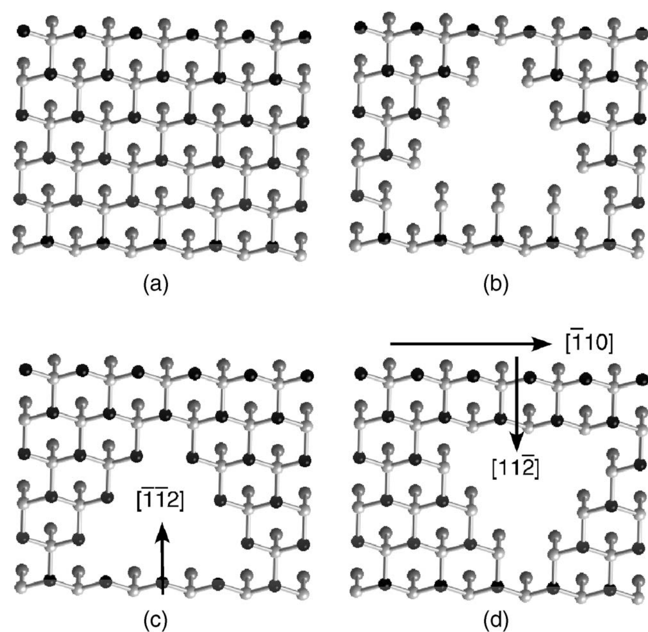

Figure 7. (a) The unreconstructed (111) plane of the diamond lattice has a surface that is composed of a bilayer consisting of upper atoms that are threefold coordinated, which have one dangling bond, and lower atoms that are fourfold coordinated because they are also bound to one atom in the layer below them. (b) Positive trigon formed when the upper bilayer atom is removed from the edge. A twofold lower bilayer atom remains on the edge. (c) Positive trigon formed when the lower bilayer atom is removed from the edge. A twofold upper bilayer atom remains on the edge. (d) Negative trigon formed when the upper bilayer atom is removed from the edge. A threefold coordinated upper bilayer atom remains on the edge.

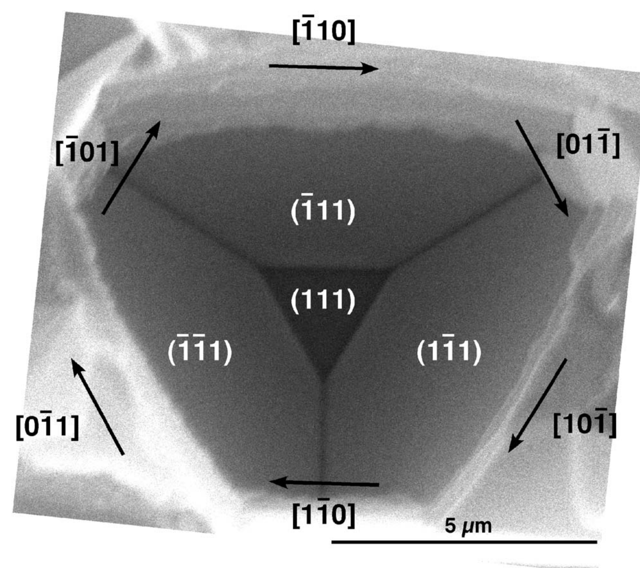

Figure 8. Crystallographic assignment of a Si(111) macropore formed from a femtosecond pillar covered substrate etched 8 min in 25 wt % TMAH at 60°C. The pore has not yet fully made the transition from hexagonal to triangular and the emergence of the three larger surviving walls with slow etching edges at the expense of the walls with fast etching edges can be observed.

positive trigon has twofold coordinated edge atoms. A negative trigon can also be formed in one of two ways by the creation of $\langle 11\bar{2}\rangle$ type steps. If a negative trigon is created by removing the lower bilayer atoms, a negative trigon with onefold coordinated atoms is formed. This is the most unstable configuration and is not shown because it will rapidly etch to form the negative trigon shown in Fig. 7d. In Fig. 7d, the etch pit that is formed by removing the upper bilayer atoms is shown. It is a negative trigon with threefold coordinated edge atoms. The kinetic stability of this structure explains the appearance of negative trigons on both etched Si(111) and natural C(111)-diamond surfaces.

Silicon, of course, also has a diamond lattice. Under anodic etching in alkaline solution, Allongue et al.[53,54] showed that the Si(111) surface is unreconstructed because it is terminated with H atoms. If we assume that this is also true for chemical etching of Si(111) in alkaline solutions at 60–80°C, then we are justified in using Fig. 7a as a starting point for our discussion of etch pit morphology for pillar-covered Si(111) wafers etched in alkaline solution. Si(111), as shown by Wind and Hines[43] and Wind et al.,[44] etches with a step-flow mechanism in hot concentrated KOH. It seems logical to postulate that steps with the lowest coordination will have the highest etch rate because these will have the least steric hindrance for forming the pentavalent transition state.[33] We therefore conclude that negative trigons are formed exclusively because they have threefold coordinated edge atoms, and these are the kinetically most stable edges. It is interesting to note that in the dry etching of Si(111) with the halogens Cl_2, Br_2, and I_2 triangular features at step edges and negative trigons are also observed under some circumstances.[55,56]

The interpillar region is highly defective and etching initially leads to the formation of rounded pores as this highly defective material is removed. Eventually, more crystallographically related features begin to appear in the form of hexagonal pores, which are composed of a superposition of positive and negative trigons. As shown in Fig. 8, the rapidly etching edges and walls of the positive trigons gradually give way and only the slower etching edges and walls of the negative trigons survive prolonged etching. The bottom of the pore is flat and parallel to the original Si(111) substrate surface; therefore, it is easily assigned as a (111) plane. This also explains why the pores attain a maximum depth. They then etch predominantly from the top because the crystallography of the top contains fast etching planes and many defects. The joints between the (111) bottom and the sidewalls appear to be sufficiently defect free that they do not readily etch compared to the top of the macropore. This is a fundamental difference between Si(001) macropores with {100} sides and Si(111) macropores. The Si(001) macropores etch significantly more in depth because the Si(001) plane etches more rapidly than Si(111), and/or there is more etching at the intersection of the sidewalls and the bottom.

To ascertain the depth of the pores as well as the orientation of the sidewalls, we aligned the pores in an orientation equivalent to that shown in Fig. 8 and then tilted the sample in steps of 1–2°, taking an image at each tilt until the lower wall was perpendicular to the viewing direction or even to the point where the bottom was obscured. We then measured the apparent length of the wall and how far the edge of the triangle at the bottom had moved at each angle. Using trigonometry, we were then able to determine the inclination between the sidewall and the bottom (111) plane as well as the height of the sidewall. Several pores have been analyzed in this fashion and resulted in sidewall-to-(111) angles varying between 67 and 70°. Analysis reveals that this angle is only consistent with an assignment of {111} planes for the sidewalls. The typical depth of the pores with well-developed {111} sidewalls is ~6 μm; however, by the time the flat {111} bottom and sidewalls appear, it is likely that the pores are already beginning to become shallower than their maximum depth.

We note here that the clear and exclusive preference for {111} sidewalls distinguishes the etch pits formed in silicon from the trigons formed by the etching of dislocations on natural diamond. For diamond,[49,50,57] a range of sidewall angles and, therefore, orientations are observed.

Downloaded on 2013-12-02 to IP 144.26.117.20 address. Redistribution subject to ECS license or copyright; see ecsdl.org/site/terms_use

Conclusion

Pillar-covered Si surfaces can be etched to reveal crystallographically defined macropores. Either rectangular pores with vertical walls or octagonal pores with irregular walls are obtained on Si(001) based on the etchant composition, whereas hexagonal or triangular pores appear on Si(111) based primarily on the extent of etching. We have assigned the crystal plane structure of the bottoms and sidewalls. Long (several micrometer), straight ridges projected along defined crystallographic directions are often observed, particularly for Si(111), and these ridges commonly have a thickness of <100 nm at their summits. The regularity, order, and spacing of the macropores is determined by the positioning of the pillars; therefore, because methods of forming ordered arrays of pillars have been demonstrated,[23,41,58] we will also be able to control the order and spacing of the macropores in addition to their shape. Macropores etched on Si(111) exhibit exclusively a negative trigon orientation, which can be explained because the edge atoms in such an etch pit have the highest coordination number and therefore are the most stable kinetically.

Acknowledgments

We acknowledge the assistance of David Mills and Barada Nayak, who helped with the production of the nanosecond and femtosecond pillar samples, respectively. We also thank Frederick Monson for his expert assistance with the SEM. This work was supported by West Chester University and the National Science Foundation under the CREST supplement program grant no. 0520208. K.W.K. is grateful for the support of Eckart Hasselbrink under Sonderforschungsbereich 616 "Energiedissipation an Oberflächen" for a research fellowship and stimulating discussions.

West Chester University assisted in meeting the publication costs of this article.

References

1. K. W. Kolasinski, *Curr. Opin. Solid State Mater. Sci.*, **10**, 182 (2006).
2. W. Lu and C. M. Lieber, *J. Phys. D*, **39**, R387 (2006).
3. H. Dai, *Surf. Sci.*, **500**, 218 (2002).
4. K. W. Kolasinski, *Curr. Opin. Solid State Mater. Sci.*, **9**, 73 (2005).
5. H. Masuda and K. Fukuda, *Science*, **268**, 1466 (1995).
6. A. G. Cullis, L. T. Canham, and P. D. J. Calcott, *J. Appl. Phys.*, **82**, 909 (1997).
7. N. W. Ockwig, O. Delgado-Friedrichs, M. O'Keeffe, and O. M. Yaghi, *Acc. Chem. Res.*, **38**, 176 (2005).
8. J. L. C. Rowsell and O. M. Yaghi, *Microporous Mesoporous Mater.*, **73**, 3 (2004).
9. A. Ramanan and M. S. Whittingham, *Cryst. Growth Des.*, **6**, 2419 (2006).
10. K. W. Kolasinski, D. Mills, and M. Nahidi, *J. Vac. Sci. Technol. A*, **24**, 1474 (2006).
11. K. Luterova, M. Cazzanelli, J. P. Likforman, D. Navarro, J. Valenta, T. Ostatnicky, K. Dohnalova, S. Cheylan, P. Gilliot, B. Honerlage, et al., *Opt. Mater. (Amsterdam, Neth.)*, **27**, 750 (2005).
12. P. M. Fauchet, J. Ruan, H. Chen, L. Pavesi, L. Dal Negro, M. Cazzaneli, R. G. Elliman, N. Smith, M. Samoc, and B. Luther-Davies, *Opt. Mater. (Amsterdam, Neth.)*, **27**, 745 (2005).
13. S. G. Cloutier, P. A. Kossyrev, and J. Xu, *Nat. Mater.*, **4**, 887 (2005).
14. J. Ruan, P. M. Fauchet, L. Dal Negro, M. Cazzanelli, and L. Pavesi, *Appl. Phys. Lett.*, **83**, 5479 (2003).
15. L. Pavesi, L. Dal Negro, C. Mazzoleni, G. Franzó, and F. Priolo, *Nature (London)*, **408**, 440 (2000).
16. O. Bisi, S. Ossicini, and L. Pavesi, *Surf. Sci. Rep.*, **38**, 1 (2000).
17. O. Boyraz and B. Jalali, *Opt. Express*, **12**, 5269 (2004).
18. H. S. Rong, R. Jones, A. S. Liu, O. Cohen, D. Hak, A. Fang, and M. Paniccia, *Nature (London)*, **433**, 725 (2005).
19. H. S. Rong, A. S. Liu, R. Jones, O. Cohen, D. Hak, R. Nicolaescu, A. Fang, and M. Paniccia, *Nature (London)*, **433**, 292 (2005).
20. M. A. Sheehy, L. Winston, J. E. Carey, C. A. Friend, and E. Mazur, *Chem. Mater.*, **17**, 3582 (2005).
21. R. Younkin, J. E. Carey, E. Mazur, J. A. Levinson, and C. M. Friend, *J. Appl. Phys.*, **93**, 2626 (2003).
22. K. W. Kolasinski, M. E. Dudley, B. K. Nayak, and M. C. Gupta, *Proc. SPIE*, **6586**, 65860H (2007).
23. D. Riedel, J. L. Hernández-Pozos, K. W. Kolasinski, and R. E. Palmer, *Appl. Phys. A: Mater. Sci. Process.*, **78**, 381 (2004).
24. F. Secco d'Aragona, *J. Electrochem. Soc.*, **119**, 948 (1972).
25. E. Sirtl and A. Adler, *Z. Metallkd.*, **52**, 529 (1961).
26. R. B. Heimann, in *Silicon Chemical Etching*, J. Grabmaier, Editor, p. 173, Spring-Verlag, Berlin (1982).
27. P. Campbell, S. R. Wenham, and M. A. Green, *Sol. Energy Mater. Sol. Cells*, **31**, 133 (1993).
28. J. D. Hylton, A. R. Burgers, and W. C. Sinke, *J. Electrochem. Soc.*, **151**, G408 (2004).
29. Z. Xi, D. Yang, W. Dan, C. Jun, and X. Li, *Semicond. Sci. Technol.*, **19**, 485 (2004).
30. F. Llopis and I. Tobías, *Prog. Photovoltaics*, **13**, 27 (2005).
31. M. M. Hilali, K. Nakayashiki, A. Ebong, and A. Rohatgi, *Prog. Photovoltaics*, **14**, 135 (2006).
32. D. S. Ruby, S. H. Zaidi, S. Narayanan, B. M. Damiani, and A. Rohatgi, *Sol. Energy Mater. Sol. Cells*, **74**, 133 (2002).
33. M. A. Hines, *Annu. Rev. Phys. Chem.*, **54**, 29 (2003).
34. J. J. Kelly and H. G. G. Philipsen, *Curr. Opin. Solid State Mater. Sci.*, **9**, 84 (2005).
35. M. A. Hines, Y. J. Chabal, T. D. Harris, and A. L. Harris, *J. Chem. Phys.*, **101**, 8055 (1994).
36. T. Baum and D. J. Schiffrin, *J. Chem. Soc., Faraday Trans.*, **94**, 691 (1998).
37. A.-S. Andersson, F. Bäckhed, A. von Euler, A. Richter-Dahlfors, D. Sutherland, and B. Kasemo, *Biomaterials*, **24**, 3427 (2003).
38. H. G. Craighead, C. D. James, and A. M. P. Turner, *Curr. Opin. Solid State Mater. Sci.*, **5**, 177 (2001).
39. E. A. Evans and D. A. Calderwood, *Science*, **316**, 1148 (2007).
40. D. Mills and K. W. Kolasinski, *J. Vac. Sci. Technol. A*, **22**, 1647 (2004).
41. D. Mills and K. W. Kolasinski, *J. Phys. D*, **38**, 632 (2005).
42. B. K. Nayak, M. C. Gupta, and K. W. Kolasinski, *Appl. Surf. Sci.*, **253**, 6580 (2007).
43. R. A. Wind and M. A. Hines, *Surf. Sci.*, **460**, 21 (2000).
44. R. A. Wind, H. Jones, M. J. Little, and M. A. Hines, *J. Phys. Chem. B*, **106**, 1557 (2002).
45. I. Zubel and M. Kramkowska, *Sens. Actuators, A*, **93**, 138 (2001).
46. I. Zubel and M. Kramkowska, *Sens. Actuators, A*, **101**, 255 (2002).
47. D. Mills, M. Nahidi, and K. W. Kolasinski, *Phys. Status Solidi A*, **202**, 1422 (2005).
48. F. M. Ross, G. Oskam, P. C. Searson, J. M. Macaulay, and J. A. Liddle, *Philos. Mag. A*, **75**, 525 (1997).
49. F. C. Frank, K. E. Puttick, and E. M. Wilks, *Philos. Mag.*, **3**, 1262 (1958).
50. J. C. Angus and T. J. Dyble, *Surf. Sci.*, **50**, 157 (1975).
51. J. Flidr, Y.-C. Huang, and M. A. Hines, *J. Chem. Phys.*, **111**, 6970 (1999).
52. J. Flidr, Y. C. Huang, T. A. Newton, and M. A. Hines, *J. Chem. Phys.*, **108**, 5542 (1998).
53. P. Allongue, V. Costa-Kieling, and H. Gerischer, *J. Electrochem. Soc.*, **140**, 1018 (1993).
54. P. Allongue, V. Costa-Kieling, and H. Gerischer, *J. Electrochem. Soc.*, **140**, 1009 (1993).
55. R. J. Pechman, X.-S. Wang, and J. H. Weaver, *Phys. Rev. B*, **52**, 11412 (1995).
56. B. S. Itchkawitz, M. T. McEllistrem, and J. J. Boland, *Phys. Rev. Lett.*, **78**, 98 (1997).
57. E. van Veenendaal, F. K. de Theije, J. van Suchtelen, and W. J. P. van Enckevort, *Diamond Relat. Mater.*, **11**, 145 (2002).
58. M. Y. Shen, C. H. Crouch, J. E. Carey, R. Younkin, E. Mazur, M. Sheehy, and C. M. Friend, *Appl. Phys. Lett.*, **82**, 1715 (2003).

Downloaded on 2013-12-02 to IP 144.26.117.20 address. Redistribution subject to ECS license or copyright; see ecsdl.org/site/terms_use